

Magnons in a one-dimensional spin glass: The high-field and zero-field limits

I. Avgin and D. L. Huber

Department of Physics, University of Wisconsin—Madison, Madison, Wisconsin 53706

(Received 31 March 1993)

The high-field and zero-field behavior of the linearized magnetic excitations (harmonic magnons) in a one-dimensional $\pm J$ Heisenberg spin glass are studied. In the high-field limit—a field strong enough to ensure complete alignment of the ground state—the density of states (DOS), the inverse localization length (ILL), and the dynamic structure factor are calculated over the interval $-4J < E - H < 4J$ (H is applied field) by employing the coherent-exchange approximation (CEA), negative-eigenvalue counting, and matrix diagonalization. In the low-energy regime ($0.001 < E - H < 0.1J$), the CEA closely approximates the exact results reproducing, in particular, the anomalous power-law behavior of the DOS $\rho(E) \sim (E - H)^{1/3}$ and the ILL $1/L(E) \sim (E - H)^{2/3}$ for the symmetric distribution of the exchange interactions (concentration $c=0.5$). In zero field, the DOS and the ILL are calculated using negative-eigenvalue counting for $0 < E < 4J$ and $0.0001 < E < 0.01J$. For $c=0.5$, a connection is established between the zero-field and the high-field limits, and for other concentrations, a phenomenological approach is developed in the low-energy regime where it is found that $\rho(E) = f(c)E^{-1/3}$ and $1/L(E) = g(c)E^{2/3}$.

I. INTRODUCTION

The nature of the ground state and the ground-state dynamics of three-dimensional Heisenberg spin glasses are still demanding problems in spite of the great efforts spent to establish a satisfactory theory. Because of frustration, the ground state is highly degenerate (apart from trivial spin rotations) ruling out any standard theoretical methods established for systems with long-range order. In order to bypass this degeneracy, we recently studied a three-dimensional spin glass in the high-field limit¹—the field was assumed to be strong enough to align all the spins in the direction of the field. We used the coherent exchange approximation (CEA) and numerical simulation techniques and compared the results of two approaches in calculations of the density of states (DOS) and the dynamic structure factor.

The Heisenberg spin-glass system in more than one dimension involves considerable difficulty in both analytical and numerical treatments. However, in one dimension, the spin-glass problem even for large arrays can be exactly solved with numerical methods since the ground state is not degenerate (see below). The Hamiltonian of a one-dimensional spin glass can be investigated using various methods developed for other disordered systems²—e.g., electronic states and lattice vibrations; it is even possible to compare the spin-glass behavior with analytical results developed for other disordered systems in the limit of weak disorder.³ The calculations in the one-dimensional spin glass can also provide qualitative insight into approximate three-dimensional models.

In this paper, we studied a one-dimensional Heisenberg spin glass in the high-field and zero-field limits. In one dimension, there is no frustration so that the system has a nondegenerate (but random) ground state contrary to the three-dimensional spin glass. We first studied the problem in the high-field limit where the large Zeeman interaction overcomes the noncollinear ground state. In

this case, the system has complexity intermediate between a spin glass and a ferromagnetic system. Because the ground state is fixed, the CEA method can be used. The density of states and the inverse localization length (ILL) can be determined from negative-eigenvalue counting techniques and compared with the results of analytical methods. In the zero-field case, Stinchcombe and Pimentel⁴ studied the harmonic magnons in a one-dimensional spin glass having a symmetric distribution of the exchange interactions. They showed that in the low-energy and long-wavelength regime, the system has anomalous dispersion relation $E \propto k^{3/2}$ contrary to the hydrodynamic picture, where the dispersion relation is $E \propto k$. Boukahil and Huber³ numerically computed the DOS and the ILL for the same distribution of the exchange interactions and formally connecting the spin glass to the one-dimensional discretized Schrödinger equation; they showed that the DOS is consistent with the pronounced anomalous dispersion relation. Here, we carry out computations for asymmetric as well as symmetric distributions of the exchange interactions. We show that for the symmetric distribution of exchange integrals the behavior in the high-field limit is equivalent to that in zero field. Developing a phenomenological method, we found the following relations in the low energy regime in zero field: the integrated density of states, integrated DOS, $I(E) = f(c)E^{2/3}$, and the ILL $1/L(E) = g(c)E^{2/3}$, where c is the concentration of the exchange interactions. Note that the CEA cannot be used in the zero-field case since the ground state is random.

A one-dimensional Heisenberg nearest-neighbor $\pm J$ spin glass can be described by the following Hamiltonian:

$$\mathcal{H} = -H \sum_n S_n^z - \sum_n J_{n,n+1} \mathbf{S}_n \cdot \mathbf{S}_{n+1}, \quad (1)$$

where H is the applied field (in units of $g\mu_B$). The exchange interaction $J_{n,n+1}$ takes on the values $\pm J$ ($J=1$)

with probability $1-c$ and the value $-J(=-1)$ with probability c , and there is no correlation between different bonds, that is, the probability distribution of $J_{n,n+1}$ has the form

$$P(J_{n,n+1}) = (1-c)\delta(J_{n,n+1}-J) + c\delta(J_{n,n+1}+J). \quad (2)$$

Note that $c=0$ describes the ideal ferromagnet, whereas, $c=1$ describes the ideal antiferromagnet. When the field $H \gg J$, the ground state is in perfect alignment, i.e., $\langle S_n^z \rangle = S$ for every lattice point n (S is the magnitude of the spin). However, for the zero-field case, $\langle S_n^z \rangle$ is random dependent on the distribution of $J_{n,n+1}$. The linearized equation of motion for the operator $S_n^+ (= S_n^x + S_n^y)$ can be written

$$i \frac{d}{dt} S_n^+ = (H + S_{n+1}^z J_{n,n+1} + S_{n-1}^z J_{n-1,n}) S_n^+ - S_n^z (J_{n,n+1} S_{n+1}^+ + J_{n-1,n} S_{n-1}^+) \quad (3)$$

(in units where $\hbar=1$). Postulating a harmonic time dependence $S_n^+ \sim e^{-iEt}$, Eq. (3) can be written

$$(E - U_n) S_n^+ = -S_n^z (J_{n,n+1} S_{n+1}^+ + J_{n-1,n} S_{n-1}^+), \quad (4)$$

where

$$U_n \equiv S_n^z J_{n,n+1} + S_{n-1}^z J_{n-1,n}. \quad (5)$$

From this set of equations, we can build a tridiagonal dynamic matrix whose eigenvalues are the magnon energies. Thus the problem is reduced to a set of equations that are coupled by the Hamiltonian in a simple manner. In the high-field limit, the dynamic matrix is symmetric.

The integrated DOS, the DOS, the ILL, and the dynamic structure factor can be obtained by solving Eq. (4). The dynamic structure factor, which is related to the inelastic neutron cross section, can be determined from the eigenvalues E_ν and eigenstates ν of the dynamic matrix by means of the following equation:⁵

$$S(Q, E) = 2\pi \sum_n \sum_\nu \delta(E - E_\nu) |\langle \nu | S_n^+ | 0 \rangle \exp(-iQn)|^2. \quad (6)$$

In our calculations, the delta function is approximated with a Gaussian with an adjustable width.

II. LYAPUNOV EXPONENT

The complex Lyapunov exponent has been fruitfully used in understanding the spectrum of the electronic disorder problem where the product of the random matrices also arises.² It provides information about the integrated DOS and the ILL. However, there is no analytical expression, even in one dimension, for the general Lyapunov exponent, except in some limiting cases, e.g., the weak disorder limit. An analysis of the Lyapunov exponents for the one-dimensional Heisenberg spin glass in the high field and zero field is made in Refs. 3 and 5.

With proper transformation (see Appendix A), Eq. (4) can be reduced to the form

$$(2 - \xi_n W) u_n = u_{n+1} + u_{n-1}, \quad (7)$$

where for the high-field case, $W = E - H$ and $\xi_n = J_{n,n+1}$, and for the zero-field case, $W = E$ and $\xi_n \equiv \prod_{i=1}^n J_{i,i+1}$. In both cases, $|J_{n,n+1}| = 1$. The respective definitions of the u_n are given in Appendix A. The difference between the high-field and the zero-field limits is reflected in the random number given above. Equation (7) is similar to that of one-dimensional discretized Schrödinger equation with a random potential (see Ref. 3).

The complex Lyapunov exponent is given in terms of the amplitude ratios by the equation

$$\gamma(W) \equiv \frac{1}{N} \sum_{n=1}^N \ln R_n, \quad (8)$$

where N is the number of the spins in the chain and amplitude ratios R_n are given by

$$R_n \equiv \frac{u_n}{u_{n-1}} (u_0 = 1). \quad (9)$$

The real part of the Lyapunov exponent

$$\text{Re} \gamma = \frac{1}{N} \sum_{n=1}^N \ln |R_n| \quad (10)$$

is the ILL (in units of reciprocal of the lattice constant) as shown by Thouless.⁶ The ILL gives information about the spatial extension of the magnon excitations. If it is zero, then the excitations are extended throughout the chain; otherwise, the excitations are localized.

The imaginary part of the Lyapunov exponent is

$$\text{Im} \gamma = \frac{\pi}{N} \sum_{n=1}^N s_n, \quad (11)$$

where

$$s_n = \begin{cases} 1 & \text{if } s_n < 0 \\ 0, & \text{otherwise} \end{cases}.$$

$\text{Im} \gamma$ is related to the integrated DOS in the electronic problem. This is the consequence of the negative-eigenvalue counting method developed by Dean.⁷ Using arguments similar to those developed for the disordered antiferromagnets,⁸ $\text{Im} \gamma$ can also be shown to give the integrated DOS for the spin-glass problem.

III. COHERENT EXCHANGE APPROXIMATION

The coherent exchange approximation (CEA), another version of the coherent potential approximation for random alloys, was introduced by Tahir-Kheli⁹ who applied it to the dilute ferromagnets and antiferromagnets. However, this method can only be applied to systems with known ground states, which in the spin-glass case is the high-field limit. According to this method, the configurational averaged Green's function at zero temperature is given by

$$\langle G(W, Q) \rangle = [W - J_c(W) S_z (1 - \gamma_Q)]^{-1}, \quad (12)$$

where $W = E - H$, $z =$ number of nearest neighbors, and $\gamma_Q = \cos Q$ (in one dimension). The coherent exchange in-

tegral characterizing the reduced random medium $J_c(W)$ is calculated self-consistently from

$$\int dJ P(J - J_c(W)) / \{1 - [J - J_c(W)] \times [W \langle G_0(W) \rangle - 1] / J_c(W)\} = 0, \quad (13)$$

where the distribution of the bonds $P(J)$ is given in Eq. (2), and the zeroth-order Green's function is

$$\langle G_0(W) \rangle = \frac{1}{N} \sum_Q \langle G(W, Q) \rangle = [(W - 2J_c)^2 - (2J_c)^2]^{-1/2}. \quad (14)$$

After solving $J_c(W)$ from Eq. (13), we can calculate the DOS and the dynamic structure factor by means of

$$\rho(W) = -\frac{1}{\pi} \text{Im} \langle G_0(W + i\epsilon) \rangle \quad (15)$$

and

$$S(Q, W) = -\frac{1}{\pi} \text{Im} \langle G(W + i\alpha, Q) \rangle, \quad (16)$$

respectively. The imaginary part of W , α , is set equal to the root-mean-square width of the Gaussian, i.e., $(2\pi\alpha^2)^{-1/2} \exp[-(E - E_v)^2 / 2\alpha^2]$ which is an approximate substitution for the delta function in Eq. (6). The ILL is given in terms of the real part of the Green's function by the equation^{5,6}

$$1/L(W) = \int dy \rho(y) \ln |W - y| = \int_0^W dx \text{Re} \langle G_0(x) \rangle, \quad (17)$$

because differentiation of the integral over y with respect to W yields $\text{Re} \langle G_0(W) \rangle$.

IV. RESULTS IN THE HIGH-FIELD LIMIT FOR THE ENTIRE SPECTRUM

In this section, the numerical and analytical results in the high-field limit are presented for the entire spectrum. The bandwidth for spin glass in this limit is 8 (in units of J) contrary to the zero-field ferromagnetic and antiferromagnetic cases where the bandwidths are equal to 4 and 2, respectively. This is the effect of the high field since for the homogeneous interactions, i.e., $c=0$ or $c=1$, an eigenvalue is between 0 and 4 or -4 and 0, respectively, and for the inhomogeneous case, it can take any value between -4 and 4. The numerical results are presented for the concentrations $c=0.1, 0.2, 0.3, 0.4$, and 0.5 with an array of size of 10^7 . Note that the results for $c > 0.5$ can be obtained from the data for $c < 0.5$ by reflection about $W=0$ ($E=H$).

The numerical results shown in Fig. 1 display rather detailed structures with dips and peaks. For $c > 0.1$, gaps develop in the DOS particularly for W values $2.0 < W < 2.1$. As the concentration increases, the modes move towards the lower edge of the spectrum, and the heights of the peaks decrease, but for all concentrations the peaks at $W=0$ maintain their heights and positions more persistently than the other peaks in the DOS. For $c=0.5$, the modes are symmetrically distributed about

$W=0$ since, for this case, the exchange integral takes on \pm values with equal probability.

The CEA curves shown in Fig. 2 for the DOS do not give all the details of the histograms but correctly predict the qualitative features. This is expected since the CEA, a mean-field-like theory, can reproduce only the average behavior. However, surprisingly, for W close to 0—corresponding to long-wavelength excitations—the CEA and the numerical results appear to be in good agreement. The high-resolution studies in the next section show that this agreement is indeed very good.

The inverse localization lengths (ILL) for concentrations are shown in Fig. 3 for $c=0.1, 0.2, 0.3, 0.4$, and 0.5. For the pure system, $c=0$ or 1, the ILL is zero, that is, all the magnon modes are extended throughout all the sites. However, for finite concentrations, the ILL takes a finite value corresponding to localization. Figure 3 shows that all the modes for $W < 0$ are heavily damped. The modes for small positive W are less localized than any other modes in the spectrum. The localization of the modes starts growing as the concentration increases.

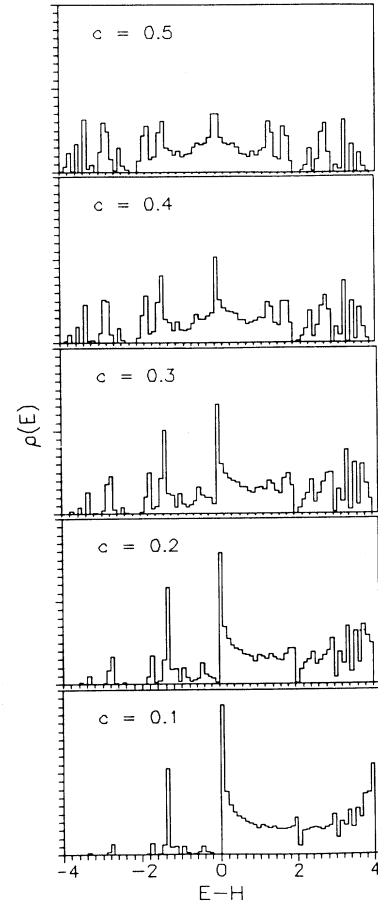


FIG. 1. Histograms of the density of states for the high-field limit for a chain of 10^7 spins for various concentrations of negative, $-J$, bonds. $J=S=1$. All the histograms have a unit area and energy is measured in units of J .

These results are in accord with the predictions of the theoretical investigations of one-dimensional disordered systems where (essentially) all the modes in one dimension are localized for any finite concentration of impurities.

Figure 4 shows the dynamic structure factors for the various concentrations for the following Q values: $\pi/4$, $\pi/2$, $3\pi/4$, and π . The numerical computations involve diagonalization of a 650×650 tridiagonal dynamic matrix. Due to the finite size of the array, the delta function in Eq. (6) is replaced by a Gaussian function with a width $\sigma (= \alpha) = 0.2$ centered at E_v . In the CEA analysis $\text{Im}W$ is set equal to σ .

With increasing c , the peaks broaden and shift towards the low-energy edge of the band. The broadening of the peaks reflects the fact that Q is not a good quantum number indicating the absence of the translational invariance. For $c < 0.4$, the peaks with higher Q values are damped less than those peaks with small Q . For $c < 0.2$, some small tails are developing on the low-energy side which eventually become satellites. As the concentration in-

creases, these satellites grow and become symmetric at $c = 0.5$ (in the thermodynamic limit).

The CEA curves evidently give the primary peak positions quite accurately as well as the shifts towards the lower edge of the band and the broadening with increasing concentration (see Fig. 5). The CEA also predicts the development of the satellites with increasing c and the symmetric peaks at $c = 0.5$. It does not reproduce any other features of the peaks and for $W = 0$, it gives minima quite contrary to numerical data.

V. HIGH-RESOLUTION STUDIES IN THE HIGH-FIELD LIMIT

As we mentioned before, the CEA results are in good agreement with the numerical data at low energies. We studied in great detail the energy interval $0 < W < 0.1$ using the CEA. Numerical data were obtained for an array of 10^7 spins for two regions of energy: $0.01 < W < 0.1$ and $0.001 < W < 0.01$ at intervals of 0.01 and 0.001, respectively.

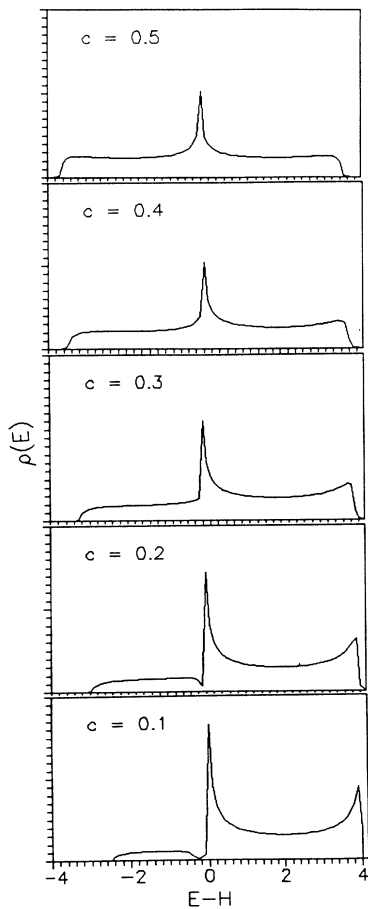


FIG. 2. Density of states obtained from the coherent exchange approximation for various values of c . All curves have the unit area and the imaginary part of the energy $\epsilon = 0.015$ and $J = S = 1$. The curves are to be compared with the corresponding histograms shown in Fig. 1. Energy is measured in units of J .

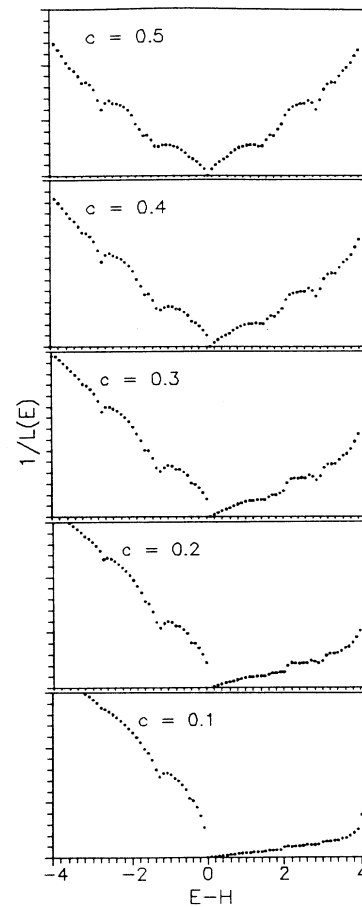


FIG. 3. The inverse localization length (ILL) for a chain of 10^7 for various concentrations of negative sign bonds. The ILL is measured in units of the reciprocal of the lattice constant. $J = S = 1$ and energy is measured in units of J .

For small W , the Green's function [Eq. (14)] assumes the form

$$\langle G_0(W) \rangle \cong -(-4J_c W)^{-1/2} \quad (18)$$

and the self-consistent equation [Eq. (13)] is written

$$\sqrt{W}(J_c^2 - 1) + 2i(\mu J_c^{3/2} - J_c^{1/2}) = 0, \quad (19)$$

where the mean of the exchange interactions $\mu \equiv \langle J_{n,n+1} \rangle = 1 - 2c$ ($J=1$). For $c=0.5$ (notice that $\mu=0$), Eq. (19) has a rather simple solution

$$J_c \cong \left[\frac{-4}{W} \right]^{1/3}. \quad (20)$$

Then, we can calculate the integrated DOS, the ILL, and the DOS (see Ref. 5 for details) which are

$$I(W) \equiv \text{Im}\gamma(W)/\pi \cong \frac{3}{\pi} 2^{-7/3} \sin \frac{2\pi}{3} W^{2/3} = 0.164 W^{2/3}, \quad (21)$$

$$1/L(W) \equiv \text{Re}\gamma(W) \cong 3/2^{7/3} \sin \frac{2\pi}{3} W^{2/3} = 0.2976 W^{2/3}, \quad (22)$$

$$\rho(W) \equiv \frac{1}{\pi} \frac{d}{dW} \text{Im}\gamma(W) \cong 0.10944 W^{-1/3}, \quad (23)$$

respectively. These results are very close to the rigorous results that were calculated in Ref. 2 for the equivalent electronic disorder problem for which the anomalous power-law behavior occurs, i.e., when the mean of the random potential is zero. The Derrida-Gardner² results for the integrated DOS, the ILL, and the DOS are written

$$I(W) = \frac{3}{\sqrt{2\pi} 6^{1/6} \Gamma(1/6)} W^{2/3} = 0.1595 \dots W^{2/3}, \quad (24)$$

$$1/L(W) = \frac{\sqrt{\pi} 6^{1/3}}{2\Gamma(1/6)} W^{2/3} = 0.2893 \dots W^{2/3}, \quad (25)$$

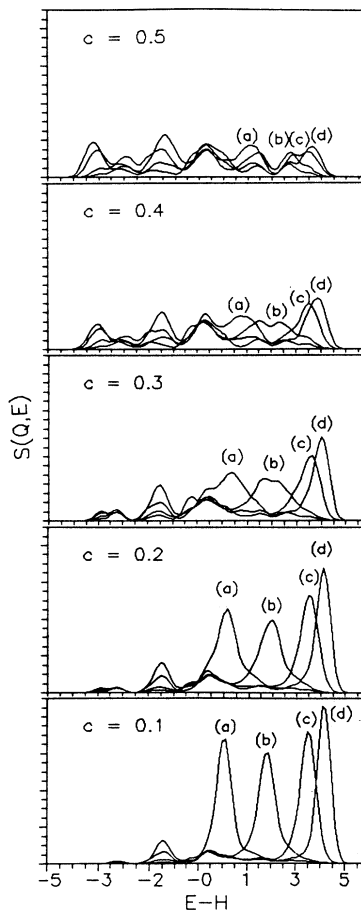


FIG. 4. Dynamic structure factors for various values of c . The curves correspond to $Q = n\pi/4$, where $n = 1$ (a), 2 (b), 3 (c), 4 (d). Data are from the diagonalization of a 650×650 tridiagonal matrix. All the curves have the same area and are calculated from Eq. (6) with $\sigma=0.2$. Energy is measured in units of J ($=S=1$).

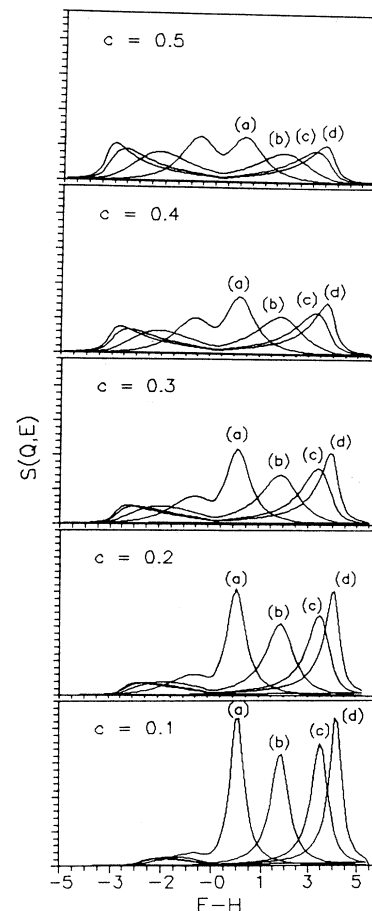


FIG. 5. Dynamic structure factors obtained from the coherent exchange approximation for various values of c . The curves correspond to $Q = n\pi/4$, where $n = 1$ (a), 2 (b), 3 (c), 4 (d). All the curves have the same area and are calculated from Eq. (16) with $\alpha=0.2$. Energy is measured in units of J ($=S=1$).

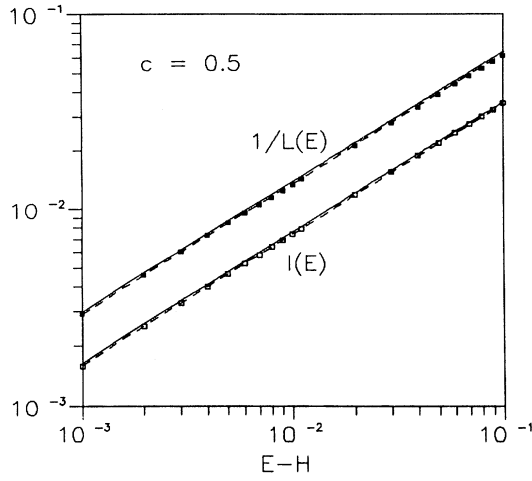


FIG. 6. The integrated density of states and the inverse localization length for $c=0.5$. The solid line represents the coherent exchange results, the dashed line is the exact calculation of Derrida and Gardner, and the symbols represent the data. The calculations are carried out for E values within these intervals: $[0.001, 0.01]$ and $[0.01, 0.1]$ for a chain of 10^7 spins. The energy is measured in units of J ($=S=1$).

$$\rho(W) = -\frac{d}{dW} I(W) = 0.10944 \cdots W^{-1/3}, \quad (26)$$

respectively, where Γ is the well-known gamma function, and we made our connection with these results using the parameters defined in Appendix A (see also Ref. 3). Figure 6 displays the CEA results, the numerical data, and the exact calculation of Ref. 2.

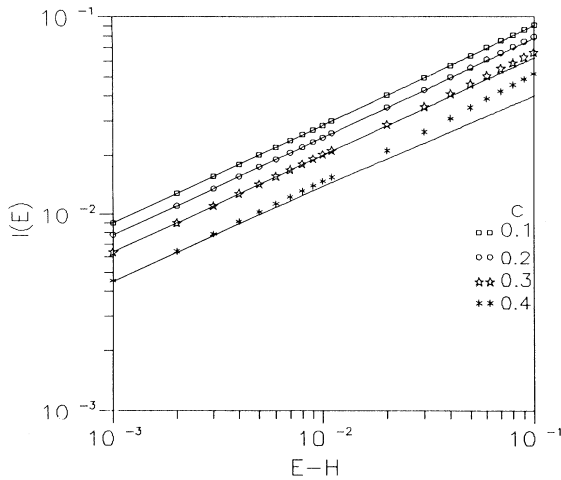


FIG. 7. The integrated density of states for various values of $c < 0.5$. The solid line represents the coherent exchange results and the symbols represent the data. The calculations are carried out for E values within these intervals: $[0.001, 0.01]$ and $[0.01, 0.1]$ for a chain of 10^7 spins, and energy is measured in units of J ($=S=1$). For $c=0.4$, the approximation breaks down for high-energy values.

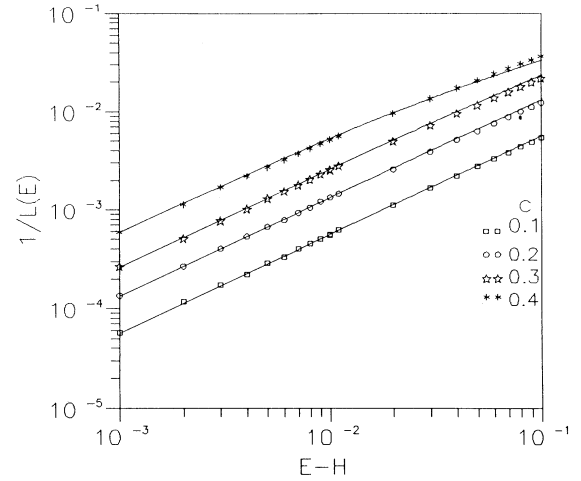


FIG. 8. The inverse localization length for various values of $c < 0.5$. The solid line represents the coherent exchange results and the symbols represent the data. The calculations are carried out for E values within these intervals: $[0.001, 0.01]$ and $[0.01, 0.1]$ for a chain of 10^7 spins, and energy is measured in units of J ($=S=1$).

For an asymmetric distribution of the bonds, $c < 0.5$, we obtained the integrated DOS, the ILL, and the DOS for small energy (see Appendix B):

$$I(W) \approx \frac{\sqrt{\mu}}{\pi} W^{1/2}, \quad (27)$$

$$1/L(W) \approx \frac{\delta^2}{8\mu} W, \quad (28)$$

$$\rho(W) \equiv -\frac{d}{dW} I(W) \approx \frac{\sqrt{\mu}}{2\pi} W^{-1/2}, \quad (29)$$

respectively. The mean of the interaction $\mu = 1 - 2c$ and the standard deviation is

$$\delta^2 \equiv \langle J_{n,n+1}^2 \rangle - \langle J_{n,n+1} \rangle^2 = 1 - (1 - 2c)^2. \quad (30)$$

These results are in exact agreement with the well-known theoretical studies of random chains for small energies done by Matsuda and Ishii.¹⁰ Again, the CEA reproduces the well-known results in the low-energy regime when the potential has nonzero mean. In brief, the low-lying modes are strongly influenced by the nature of the random bonds only if the mean of the interaction is zero; otherwise, the dynamics of the low-energy modes is the same as the pure system with regard to power-law behavior. The numerical and the CEA results are shown in Figs. 7 and 8. It is clear from the figures that the approximation works very well except for $c=0.4$ where the approximation starts breaking down for $W \sim 0.1$.

VI. RESULTS IN ZERO FIELD FOR THE ENTIRE SPECTRUM

This section is devoted to a presentation of the results of the spin glass in zero field over the entire spectrum. The magnons are distributed between 0 and 4 (in units of

J). In the limit of $c=0$ and 1, the spin glass reduces to a ferromagnetic or an antiferromagnetic system, respectively. In zero field, the ground state shows no long-range order, a feature which is characteristic of the spin glass. The average magnetization per site $m_z = (1/N) \sum_{n=1}^N \langle S_n^z \rangle = 0$, where $\langle \dots \rangle$ is the average over the disorder for large number of spins. The z component of the spin $S_n^z \equiv \xi_n = \prod_k^n J_{k,k+1}$ (see Appendix A).

The DOS histograms obtained by negative-eigenvalue counting for a chain of 10^7 sites at concentrations $c=0.1, 0.2, \dots$, and 0.9 are shown in Fig. 9. The histograms show very rich structure for most the concentrations. At $c=0.1$ and 0.9, the distributions resemble the distributions for a ferromagnetic and an antiferromagnet, respectively. As the concentration increases, the modes with the high and low energy move towards the energy $E=2$ (notice that $W=E$ for zero field) where the distribution of the antiferromagnetic modes has a peak. This is due to

the fact that the antiferromagnetic interactions start to dominate strongly as the number of the $-J$ interactions is increased. For $0.1 < c < 0.5$, several gaps open especially for $2 < E < 2.1$ and $3 < E < 3.1$, and for $c > 0.5$ the gaps widen until eventually all the modes are found in the interval $0 < E < 2$ ($c=1$). Although the histograms suggest that the DOS histograms assume a finite value for all concentrations and small E , the high-resolution studies revealed that the DOS diverge for all concentrations as E approaches 0.

Figure 10 shows the ILL results for all the concentrations in zero field. As apparent in the plots, all the modes are localized except for the ones at $E=0$. This is again in agreement with the fact that essentially all the modes in a one-dimensional disordered system are localized. The zero-energy mode involves simultaneous rotation of all the spins about a common angle, in which case the restoring force is zero. The low-energy modes are less

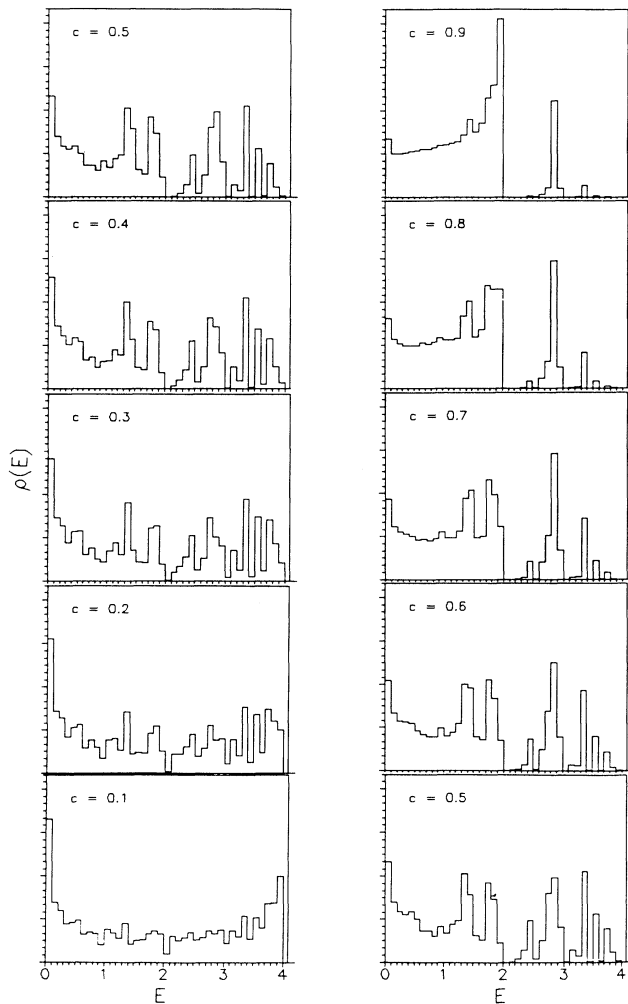


FIG. 9. Histograms of the density of states in zero-field limit for a chain of 10^7 spins for various c values. All the histograms have the unit area and energy is measured in units of J ($=S=1$).

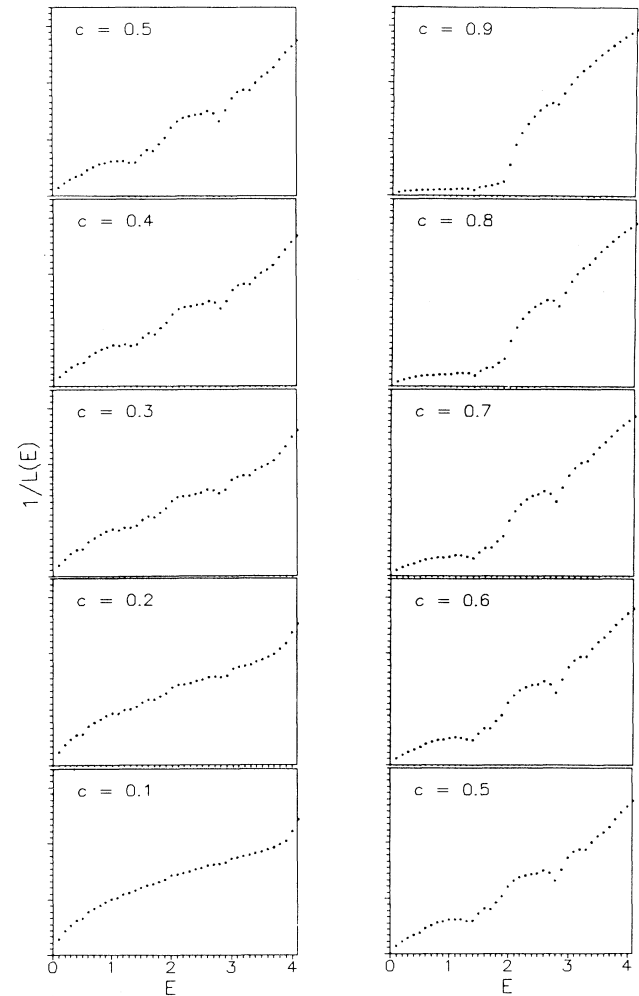


FIG. 10. The inverse localization length, in units of the reciprocal of the lattice constant, for various c values for a chain of 10^7 spins. Energy is measured in units of J ($=S=1$).

damped than those at high energy. The magnons with more ferromagnetic interactions ($c < 0.5$) are localized more strongly than those modes for $c > 0.5$. For c close to 1, a very sharp increase in the ILL is observed for $E > 2$. The ILL plot for small energy values appear to indicate different power-law behavior for different concentrations; however, as discussed below, the high-resolution studies revealed that for $E < 0.01$, the ILL for all c values have the same power-law behavior.

VII. HIGH-RESOLUTION STUDIES IN ZERO FIELD

In this section, we report the studies of the one-dimensional spin glass in zero field for asymmetric bond distributions. The numerical data of the integrated DOS and the ILL are computed for two regions of E : $0.0001 < E < 0.001$ with increments of $\delta E = 0.0001$ and $0.001 < E < 0.01$ with increments of $\delta E = 0.001$. We develop a phenomenological approach to calculate the same quantities. The numerical and the phenomenological results of the integrated DOS and the ILL are displayed in

Figs. 11 and 12.

The phenomenological equations were obtained as follows. First, we computed a "best fit" to determine power-law behavior, i.e., AE^x with A and x adjustable parameters—the method is described in Ref. 3. The estimated values of A and x are given in Table I. Table I shows that the exponents of the integrated DOS and the ILL are very close to $\frac{2}{3}$. The coefficients (A) decrease as the concentration increases for both integrated DOS and the ILL in agreement with the overall results. In the zero-field case, the anomalous power-law behavior ($\frac{2}{3}$) exists effectively for all concentrations; whereas, in the high-field limit, it exists only for the symmetric distribution of the exchange integrals. This may be connected with the fact that our numerical tests showed that the average of the random potential $U_n = (\prod_k^N J_{k,k+1})E$ taken over the sites is zero for all finite concentrations, i.e., $(1/N)\sum_n U_n = 0$. As explained earlier, the anomalous power-law behavior is seen when the average of the random potential is zero.

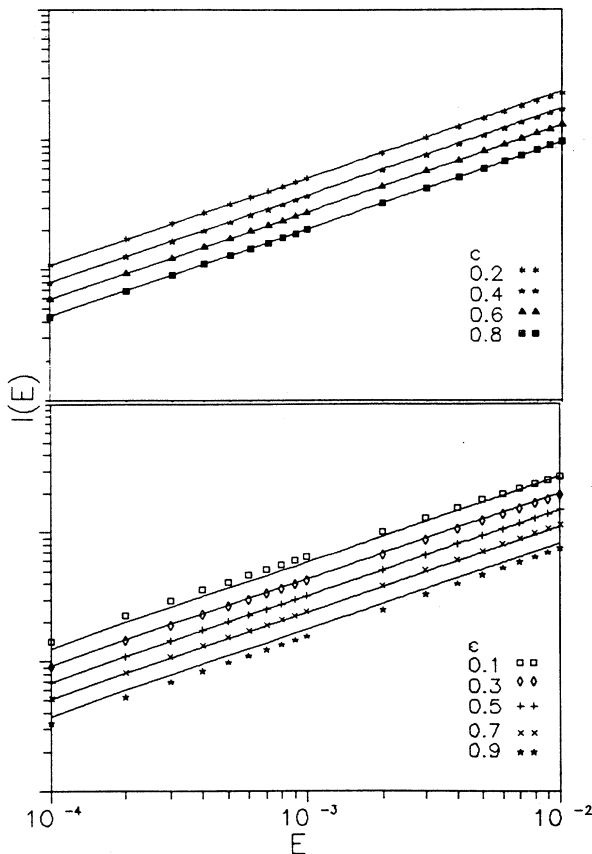


FIG. 11. The integrated density of states for various c values in the low-energy regime. The symbols are the numerical results and solid lines are the theoretical results for the phenomenological model. The calculations are carried out for E values within these intervals: $[0.0001, 0.001]$ and $[0.001, 0.01]$ for a chain of 10^7 spins, and energy is measured in units of J ($=S=1$). For $c=0.1$ and 0.9 , small deviations are due to finite-size effect.

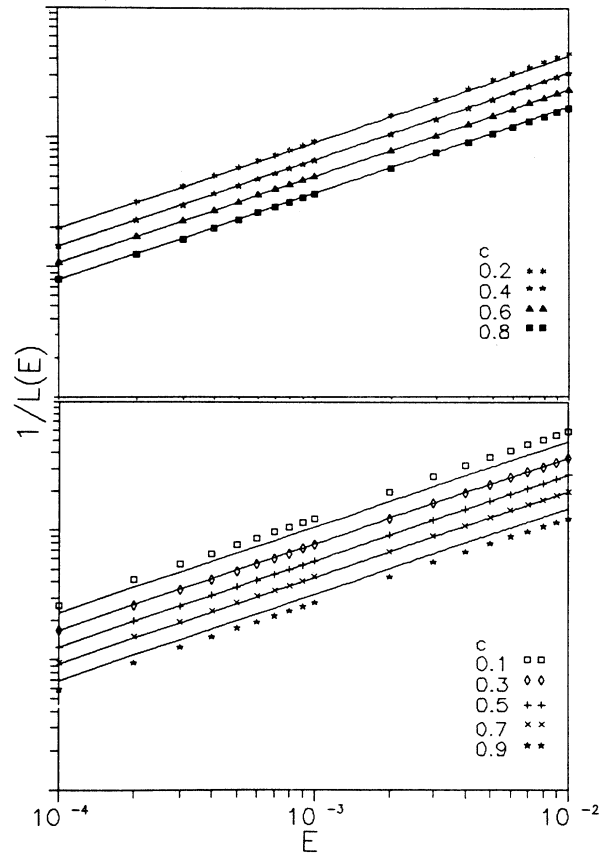


FIG. 12. The inverse localization lengths (ILL), in units of the reciprocal of the lattice constant, for various c values in the low-energy regime. The symbols are the numerical results and solid lines are the theoretical results for the phenomenological model. The calculations are carried out for E values within these intervals: $[0.0001, 0.001]$ and $[0.001, 0.01]$ for a chain of 10^7 spins, and energy is measured in units of J ($=S=1$). For $c=0.1$ and 0.9 , small deviations are due to finite-size effect.

TABLE I. The coefficient A and the exponent x of the integrated DOS and the ILL.

c	$1/(E)=\text{Re}\gamma(E)$ (ILL)		$I(E)=\text{Im}\gamma(E)$ (int. DOS)	
	A	x	A	x
0.100	0.665	0.677	0.264	0.640
0.200	0.488	0.674	0.233	0.657
0.300	0.394	0.670	0.205	0.663
0.400	0.331	0.666	0.181	0.665
0.500	0.287	0.666	0.161	0.668
0.600	0.248	0.664	0.141	0.668
0.700	0.212	0.663	0.125	0.671
0.800	0.172	0.659	0.106	0.672
0.900	0.127	0.657	0.084	0.677

Second, close examination of Table I shows that for $c=0.5$, not only $\langle U_m \rangle = 0$ but also $\langle U_m U_n \rangle = 0$ except when $n=m$. On the other hand, for all the other concentrations, $\langle U_m \rangle = (1-2c)^m \sim 0$ for $m > 2$ and $\langle U_m U_n \rangle = (1-2c)^{|m-n|}$, which is significant for the nearest-neighbor pairs (m, n) and for $m=n$. Thus, the configuration average of U_m involves a power determined by the absolute distance from the origin m ; hence, it is effectively zero. However, the correlation of $U_m U_n$ involves a power determined by the relative distance $|m-n|$ between the sites; as a result, it is large for both $n=m$ and when n and m are nearest neighbors. As indicated earlier, the existence of $(\frac{2}{3})$ power is associated with the random potential having zero mean which is shown above to be the case for all concentrations in zero field. Moreover, the Derrida-Gardner² results are analytically exact for the integrated DOS and the ILL for $c=0.5$ in the weak disorder limit and involve only the second moments, for example, $I(E) = 0.1595(\lambda^2 \langle U_m U_m \rangle)^{1/3}$, where $\lambda=1$ for the corresponding spin-glass problem. One may assume that, for the asymmetric case, terms like $\langle U_m U_n \rangle$ which are nonzero and functions of c , might contribute to the integrated DOS and the ILL. Starting from this idea, it is plausible that the integrated DOS and the ILL coefficients must be the functions of c , i.e., $I(E) = f(c)E^{2/3}$ and $1/L(E) = g(c)E^{2/3}$. For $c=0.5$ $f(0.5)$ and $g(0.5)$ are known from the Derrida-Gardner results. Taking these results as our basis, we can calculate the functional form of $f(c)$ and $g(c)$ for all c . To achieve this, we used the numerical data to calculate the ratios

$$R_i = I(E_0, c) / I(E_0, c=0.5) \quad (31)$$

and

$$R_l = L(E_0, c=0.5) / L(E_0, c) \quad (32)$$

by fixing the energy E_0 where $ef(c) = f(0.5)R_i$ and $g(c) = g(0.5)R_l$. Figure 13 shows the ratios for various values of the energy. The R_i and R_l are slightly different for different values of the energies, but both can be approximated by $2.1 \exp(-\frac{3}{2}c)$. Results of this approach and the numerical data shown in Figs. 11 and 12 are effectively in agreement except for $c=0.1$ and 0.9 where the size of the chain is probably not long enough to simulate the thermodynamic limit. Nevertheless, this ap-

proach provides an approximate formula for the density and localization of the low-lying excitations of the spin glass in the absence of a field as a function of c .

VIII. SUMMARY AND DISCUSSION

We studied the excitations in a one-dimensional $\pm J$ Heisenberg spin glass in two limits: high field and zero field. Although the one-dimensional spin glass is not a realistic model, many insights can be gained in understanding harder problems like the three-dimensional spin glass. Another advantage is that numerical results can be obtained for large arrays. In addition, there are exact theoretical calculations in one dimension. The negative-eigenvalue counting technique is used to determine the eigenvalue distributions and localization lengths while matrix diagonalization is used to calculate the dynamic structure factors. We transformed the spin equation of motion to the form of a one-dimensional discretized Schrödinger equation for which exact results have been developed in the weak disorder limit for a symmetrical distribution of the potential fluctuations.

In the first limit, we eliminated the random behavior of the ground state by means of a very strong applied field so that we are able to use the coherent exchange approxi-

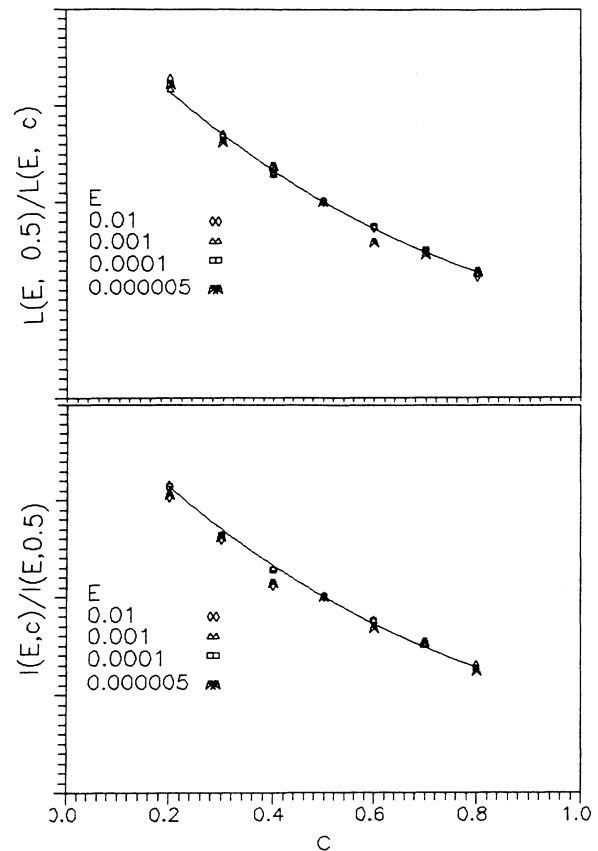


FIG. 13. The ratios given in Eqs. (31) and (32). The horizontal line is concentration c . The line represents the computer "best fit" which is found for both ratios: $2.1 \exp(-\frac{3}{2}c)$. Symbols are the ratios for a specified energy.

mation. The behavior of the spin glass in this limit is very similar to that of a diagonal electronic problem. The CEA reproduced numerical data for low energies and agreed qualitatively with the numerical data over the whole spectrum. In the case of symmetric bond distributions, the CEA successfully reproduced the anomalous power-law behavior of the integrated DOS and the ILL found in earlier calculations. We also demonstrated that for $c=0.5$, the high-field and zero-field cases are equivalent.

In zero field the ground state is random without frustration. For a low concentration of “wrong sign” bonds, the distributions are very close to the distributions in ferromagnetic and antiferromagnetic systems. In the low-energy regime, we developed a phenomenological approach based on the exact results for a symmetric distribution of bonds. We noticed that for all concentrations, the configuration average of the random potential is zero which gives rise to the $(\frac{2}{3})$ power in the integrated DOS and the ILL while the correlation of the random potential does not vanish between different sites. We then hypothesized that these nonzero correlations, which are functions of c , may cause the integrated DOS and the ILL for the asymmetric cases to differ from the symmetric case in the prefactors multiplying $E^{2/3}$. The approximation reproduced the numerical data fairly well for most of the concentrations, although slight deviations occurred for $c=0.1$ and 0.9 presumably because of finite-size effects.

The real part of the Lyapunov exponent is used to calculate the localization of the magnons. All the nonzero modes are localized confirming the long-realized-fact that all modes are localized in one dimension for any amount of disorder. Only the zero energy modes are extended since they correspond to the rotation of the spins about a common axis where there is no restoring force. The low-energy modes are the less localized than those at high energy.

Recently, Evagelou and Wang¹¹ computed the spectral properties of a spin glass using an equation equivalent to (A5) with $\lambda\beta_n = \zeta_n E$. However, they took ζ_n to be 1 with probability $1-c$ and -1 with probability c . Although not explicitly stated, their findings apply to the high-field limit (where they agree with ours), not to zero field.

Nevertheless, the excitations in the spin glass still remain a challenging problem even in one dimension. The next step is to find an approximate theory to predict the qualitative dynamical behavior of a real spin glass in zero field that gives as good results as the CEA does in the high-field limit or at least, to reproduce for c dependence of the phenomenological prefactors of the integrated DOS and the ILL analytically.

ACKNOWLEDGMENTS

We would like to thank A. Boukahil for helpful comments and for bringing Ref. 11 to our attention. Research was supported in part by the National Science Foundation.

APPENDIX A: TRANSFORMATION OF THE SPIN EQUATION OF MOTION

The equation of motion given in Eq. (4) in the high-field limit has the form

$$(E - H + J_{n,n+1} + J_{n,n-1})S_n^+ = J_{n,n+1}S_{n+1}^+ + J_{n-1,n}S_{n-1}^+ . \quad (\text{A1})$$

The z component of the spin operators are set equal to 1 because of the high field. Using the transformation¹²

$$u_n \equiv J_{n,n+1}(S_{n+1}^+ - S_n^+) \quad (\text{A2})$$

and inverse transformation

$$S_n^+ \equiv (u_n - u_{n-1})/(H - E) , \quad (\text{A3})$$

Eq. (A1) reduces to the form

$$(2 - J_{n,n+1}W)u_n = u_{n+1} + u_{n-1} , \quad (\text{A4})$$

where $W \equiv E - H$ and $J_{n,n+1}$'s are random independent variables taking values ± 1 with the probability distribution given in Eq. (2). Equation (A4) is equivalent to a site diagonal disorder form with a random potential $U_n = J_{n,n+1}W$ whose weak disorder expansion corresponds to the small-energy limit since weak disorder means in general the small fluctuations of a random potential around its average.

For the zero-field case, we can use another useful transformation of the spin operator

$$u_n \equiv \zeta_n S_n^+ \quad (\text{A5})$$

known as Mattis transformation¹³ where ζ_n is specified later. Then the equation of the motion for the spin operator Eq. (4) is written in terms of the new operators

$$(2 - \zeta_n E)u_n = u_{n-1} + u_{n+1} , \quad (\text{A6})$$

where $\zeta_{n+1} = J_{n+1}\zeta_n$ and $\langle S_n^z \rangle = \zeta_n = \pm 1$. This is again a diagonal disorder problem with a different random potential $U'_n \equiv \zeta_n E = \prod_{k=1}^n J_{k,k+1}$. The variables ζ_n are not independent but rather correlated random variables contrary to the high-field limit. This is the cause of the different behavior in the two limits. However, for a symmetric distribution of the bonds, i.e., $c=0.5$, the random potentials for both cases have similar characteristics—such as their mean and their correlation for different sites are zero—which is the reason for the appearance of the anomalous power-law behavior. Thus, both cases are equivalent for $c=0.5$.

Note that we can describe both problems with one equation with an appropriate parametrization

$$u_{n+1} + u_{n-1} - (w - \lambda\beta_n)u_n = 0 , \quad (\text{A7})$$

where $w=2$ and $\lambda\beta_n = WJ_{n,n+1}$ for the high-field limit or $\lambda\beta_n = E\zeta_n$ for the zero-field case. For the electronic problem, $w=E$, $\lambda\beta_n = U_n$, and $u_n = \Psi_n$, where U_n and u_n are the potential and the electron-wave function at the site labeled n . Through these parameters, we can adapt the spin-glass problem to other theories developed for the weak disorder limit.

APPENDIX B: SOLUTION OF THE SELF-CONSISTENT EQUATION FOR THE ASYMMETRIC CASE IN THE HIGH-FIELD LIMIT⁵

When there is an asymmetric distribution of the bonds, the self-consistent equation (19) for $W=0$ has a simple solution for the exchange integral

$$J_c(W=0) = 1/(1-2c) = 1/\mu, \quad (\text{B1})$$

where μ is the mean of the exchange integral. Equation (19) is a complex nonlinear equation for nonzero W values. However, we can solve it with a suitable approximation. Writing the coherent exchange integral in polar coordinates and inserting in Eq. (18), we get for the real and imaginary parts of the self-consistent equation

$$\sqrt{W}(R^2-1)\cos\theta - 2\sqrt{R}(\mu R+1)\sin\theta/2 = 0, \quad (\text{B2})$$

$$\sqrt{W}(R^2+1)\sin\theta + 2\sqrt{R}(\mu R-1)\cos\theta/2 = 0, \quad (\text{B3})$$

respectively, where $J_c = R \exp(i\theta)$. This set of equations is still hard to work with. The first term of the Eq. (B3) is small since $W \sim 0$ and then, if we approximate $R \approx 1/\mu$, the second term of Eq. (B3) goes to zero as well. Then, we can solve Eq. (B2) for θ by

$$x^2 + 2\frac{\mu^{3/2}}{\delta^2\sqrt{W}}x - \frac{1}{2} = 0, \quad (\text{B4})$$

where $x \equiv \sin\theta/2$ and the variance of the exchange integral $\delta^2 = 1 - \mu^2$. Having determined the coherent exchange integral in this manner, we can then calculate the integrated DOS, the ILL, and the DOS. For the detailed solution see Ref. 5.

¹I. Avgin and D. L. Huber, Phys. Rev. B **46**, 223 (1992).

²B. Derrida and E. Gardner, J. Phys (Paris) **45**, 1283 (1984).

³A. Boukahil and D. L. Huber, Phys. Rev. B **40**, 4638 (1989).

⁴R. B. Stinchcombe and I. R. Pimentel, Phys. Rev. B **38**, 4980 (1988).

⁵I. Avgin Ph.D. thesis, University of Wisconsin—Madison, 1993.

⁶D. J. Thouless, J. Phys. C **5**, 77 (1972); Phys. Rep. **13**, 93 (1974).

⁷P. Dean, Proc. Phys. Soc. London **73**, 413 (1959).

⁸D. L. Huber, Phys. Rev. B **8**, 2124 (1973).

⁹R. A. Tahir-Kheli, Phys. Rev. B **6**, 2808; **6**, 2826 (1972).

¹⁰H. Matsuda and K. Ishii, Prog. Theor. Phys. Supp. **45**, 56 (1970).

¹¹S. N. Evangelou and A. Z. Wang, J. Phys. Condens. Matter **4**, L617 (1992).

¹²D. Petris, in *Statistical Mechanics and Field Theory: Mathematical Aspects*, edited by T. C. Dorlas, N. M. Hugenholtz, and M. Winnink, Lecture Notes in Physics Vol. 257 (Springer-Verlag, New York, 1985).

¹³D. C. Mattis, Phys. Lett. **56A**, 421 (1976).